Z. Phys. B – Condensed Matter 80, 353–357 (1990)

Condensed Zeitschrift für Physik B Matter

Narrow band in the intermetallic compounds MNiSn (M = Ti, Zr, Hf)

F.G. Aliev[1], V.V. Kozyrkov[1], V.V. Moshchalkov[1], R.V. Scolozdra[1], and K. Durczewski[2]

[1] Department of Physics, Moscow State University, SU-117234 Moscow, USSR
[2] Institute for Low Temperature and Structure Research, Polish Academy of Sciences, POB937, PL-50-950 Wroclaw, Poland

Received August 1, 1989; revised version March 22, 1990

The presence of a narrow band below conduction band of nonmagnetic compounds MNiSn (M = Ti, Zr, Hf) is assumed to explain their low temperature properties such as the heat capacity, IR optics, electronics transport. A computation of the Seebeck coefficient supplies support for this assumption.

Introduction

During last few years new important physical phenomena were discovered in intermetallic compounds of MgAgAs structure [1–6]. A remarkable feature of this structure is the fact that it can be represented as consisting of the four interpenetrating cubic fcc sublattices $A(0, 0, 0)$; $B(1/4, 1/4, 1/4)$; $C(1/2, 1/2, 1/2)$ and $D(3/4, 3/4, 3/4)$, one of which, e.g. C, is empty.

In 1983 de Groot et al. showed [1] that this specific feature of MgAgAs structure in magnetic compounds (including Mn ions) may lead to an occurrence of a new class of materials – the so-called semimetallic ferromagnetics. The loss of the inversion symmetry at Mn positions and a strong interaction of the valence electrons with the magnetic sublattice can produce the full spin polarization of d-electrons at the Fermi level in the ferromagnetic state of NiMnSb and PtMnSb [1]. This suggestion was later confirmed by experiments with polarized electron beams [2]. In the nonmagnetic intermetallic compounds MNiSn (M = Ti, Zr, Hf) of this structure the vacancy sublattice produces a narrow 0.1–0.2 eV gap near Fermi level [3–5]. Very similar properties of UNiSn with MgAgAs structure [7, 8] indicate the gap existence also in this antiferromagnetic ($T_N = 47$ K) compound, though there are theoretical considerations [9] trying to describe its properties by semimetallic ferromagnetism.

The electronic specific heat of MNiSn compounds studied in our work together with transport properties and IR optics [3–5] reveal rather high effective mass of current carriers m^*, being of the order of a few free electron masses m_e. In our paper we present possible zone scheme with one or even two mobility edges E_c (in the narrow band of heavy carriers and in the conduction band), which can explain number of physical properties of these compounds. Computing of the temperature dependences of Seebeck coefficient S in one zone approximation which takes into account estimated effective mass and Hall effect data [5] is in a good correspondence with experimental S values at $(100 < T < 300)$ K.

Sample preparation

The samples were prepared by arc-melting of the stoichiometric amounts 99,99% pure constituents in the argon atmosphere. The characterization of the samples by standard X-ray diffraction technique showed that almost all the peaks were indexed as the cubic MgAgAs-type structure. In the nonannealed samples two phases exist: the stoichiometric phase MNiSn (phase I) and the Ni-defected phase $MNi_{1-x}Sn$ ($x \approx 0.04$) (phase II) with different lattice parameters a_I and a_{II} ($\Delta a \approx 0.01$ Å). The annealing in vacuum at 800 °C leads to the disappearance of the phase II. The similar properties are exhibited by UNiSn [7], where the crystallographic disorder in the Ni sublattice disappears with the annealing.

Because of the closeness of Zr and Sn atoms radii (Zr – 0.160 nm; Sn – 0.158 nm) in ZrNiSn samples, these atoms may substitute each other. In this situation the chemical formula of the annealed MNiSn compounds may be written as $Zr_{1-x}Sn_xNi(Vac)Sn_{1-x}Zr_x$ $(0.1 < x < 0.3)$ [5]. The essential difference of the Ti (0.147 nm) and Sn atoms radii makes the probability of their mutual substitution very small. So we have not found any irregularities in the position of Ti and Sn atoms in TiNiSn samples. In this case, there is no problem to prepare the monocrystalline TiNiSn, while our attempts to prepare ZrNiSn and HfNiSn monocrystals ended in failure.

The disorder in the compounds with MgAgAs-type structure was also found in a new half ionic and half covalent semiconductor LiAsZn, where Li and Zn substitutions may change low-temperature properties [6].

So the disorder in the Ni sublattice and the substitution of the Zr and Sn atoms may affect the physical properties of MNiSn compounds. To obtain more ordered crystal structure we annealed the samples for 5–30 days. More detailed information on how the annealing influences the physical properties was given in previous paper [5].

A model band structure

Figure 1 illustrates two possible band structure schemes for MNiSn compounds. In the first case (Fig. 1a) vacancy level (with capacity about $10^{22}\,cm^{-3}$), which physical origin may be caused by the vacancy sublattice in MgAgAs structure, is completely occupied and lay about 0.2 eV below mobility edge E_c of the conduction band ($E_g = E_c - E_v$). In the second case (Fig. 2b) vacancy level lay below and overlap with conduction band ($E_g = E_{c1} - E_F$). The value E_g is equal to 0.12; 0.18; 0.22 eV for TiNiSn, ZrNiSn and HfNiSn respectively [4].

Let us compare these two models with experimental data to conclude what picture is more realistic. Both models can explain finite C/T value at $T \to 0$; exponential behavior of the resistivity at $(500 < T < 1000)$ K [4] and transition from quasimetallic to Mott's behavior obtained from $\rho(T)$ at low ($T < 50$ K) temperatures [3]. In fact, this transition means that Fermi energy passes through localization edge (E_c on Fig. 1a or E_{c1} on Fig. 1b). On the other hand the absence of finite band edge in energy dependence of absorption coefficient found from IR optic experiments [4], negative sign of carriers in the whole measured temperature range obtained from thermoelectric power (see next paragraph) and Hall effect [5] could be understood only in frame of the second model.

Thus, the main properties of MNiSn compounds at temperatures less then $T = 300$ K can be described by the electrons of the narrow band of the width about a few hundred K, which is located below conduction band. The small width of the vacancy band is probably due localization of electrons in the ordered vacancy sublattice. In fact, recent investigations of the positron annihilation in NiMnSb with MgAgAs type crystal structure reveal deep potential pits at vacancy positions, being absent in the non-vacancy counterpart compound Ni_2MnSb [10].

If, only bottom of vacancy band is occupied by electrons and disorder is absent, we can assume in the first approximation the vacancy band to be parabolic. As a next approach one should take into account existence of the mobility edge E_c, caused by irregularities (partial substitution) in positions of M and Sn elements.

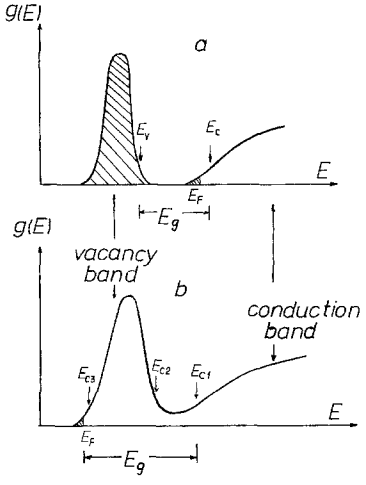

Fig. 1. Two proposed band structures of MNiSn compounds.

Heat capacity and thermoelectric power: experimental results

The high effective mass of carriers in MNiSn compounds is confirmed by the measurements of the temperature dependence of specific heat. Low temperature specific heat data for all MNiSn samples in coordinates C/T versus T^2 are represented in Figs. 2–4. We tried to fit them by the equation $C = \gamma T + \beta T^3$ to obtain values of γ and β, where γ is the electronic specific heat coefficient and the coefficient β gives the contribution due to the lattice specific heat. But only one system, namely TiNiSn, showed a good agreement with such fitting (Fig. 4). All others curves were not the strait lines in such coordi-

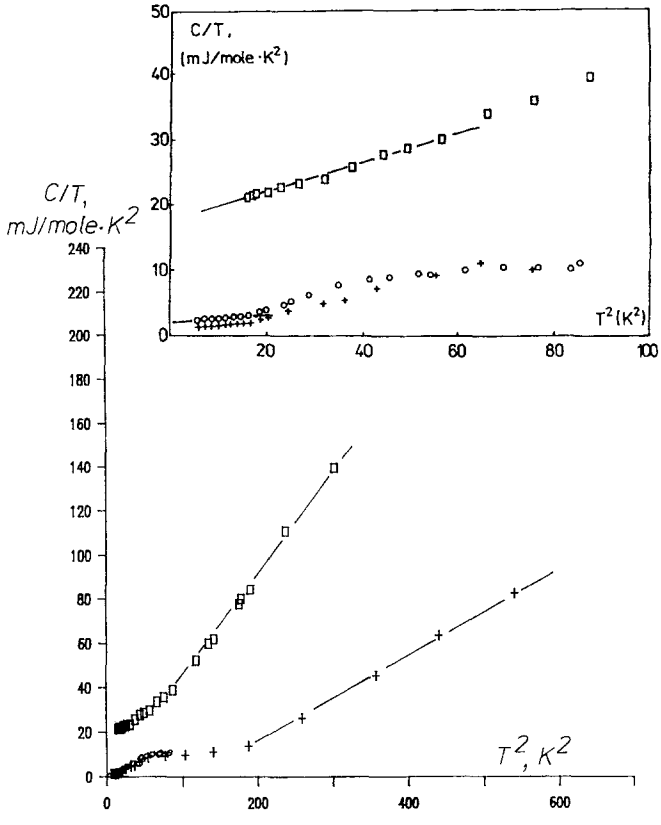

Fig. 2. Temperature dependences C/T vs T^2 for $ZrNi_2Sn$ (□) and two ZrNiSn samples – N°191c (+) and N°691 (○). Insert shows C/T vs T^2 curves at $T < 10$ K

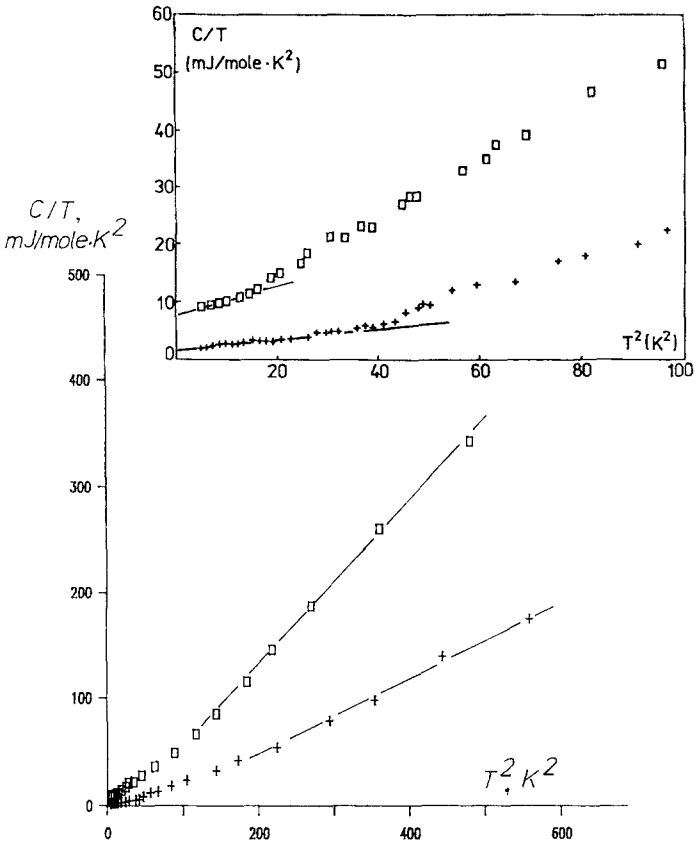

Fig. 3. Temperature dependences C/T vs T^2 for $HfNi_2Sn$ (□) and HfNiSn N° 559 (+). Insert demonstrates low temperature ($T<10$ K) data

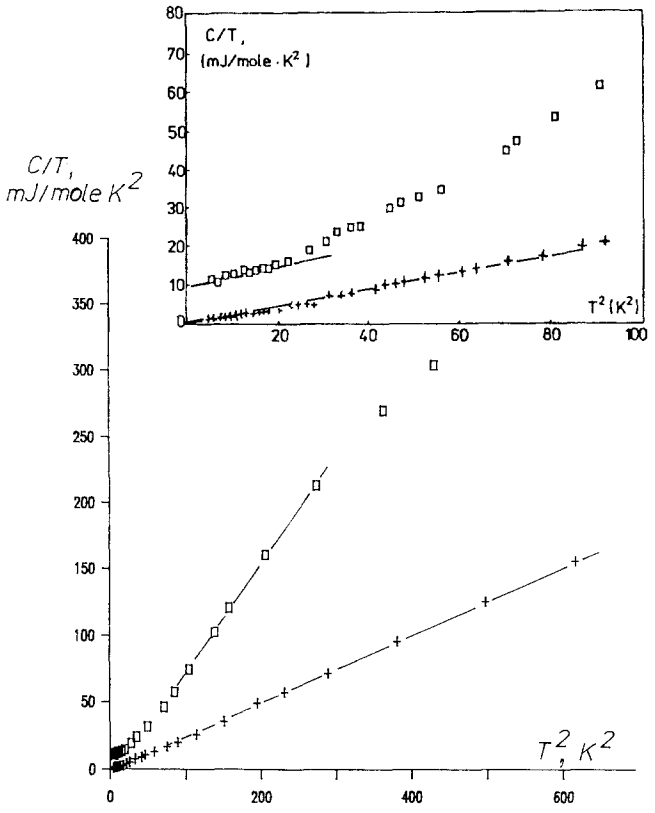

Fig. 4. Dependences C/T on T^2 for $TiNi_2Sn$ (□) and TiNiSn N° 568 (+) samples. Low temperature data are shown on the insert

nates. But since they were linear in some temperature ranges, which we pointed out by lines in the figures, we used those linear parts of curves to calculate the electronic specific heat γ by the extrapolation of C/T values to $T\to 0$, and the Debye temperature Θ_D was calculated from β in temperature range ($10\text{ K}<T<30$ K) through the equation: $\Theta_D=(12\pi^4 R/5\beta)^{1/3}$ with gas constant R. In the Table 1 we compiled the Debye temperatures Θ_D and the electronic specific heat coefficient $\gamma(T=0)$ for MNiSn (M = Ti, Zr, Hf) compounds and their nonvacancy counterparts MNi_2Sn.

The analysis of Figs. 2–4, illustrating the temperature dependence of the electron specific heat, and Table 1 shows that:

(i) $\gamma(T=0)$ in all the vacancy compounds MNiSn (M = Ti, Zr, Hf) is finite and about ten times less than the corresponding value of their nonvacancy counterparts. We believe that the rest of $C/T(T^2)$ value is due to electrons. If we estimate now the density of electron states as $g(E_F)=7.96\cdot 10^3\cdot\gamma$ [states/cm^3·erg·spin] we obtain within the parabolic band approximation the effective mass $m^*=(2-3)m_e$, provided that the density of carriers $n=n_H=10^{19}$ cm^{-3} as shown in [5]. This magnitude of m^* is in good agreement with the estimation $m^*>2m_e$ obtained early from IR spectroscopy [4, 5]. The smaller $\gamma(0)$ value found for TiNiSn in comparison with HfNiSn and ZrNiSn may be due to more ordered crystal structure in this compound and as a consequence, smaller E_F and E_c energies.

Table 1

ZrNiSn	$ZrNi_2Sn$	HfNiSn	$HfNi_2Sn$	TiNiSn	$TiNi_2Sn$
T_D[K]					
310±10	275±25	255±20	228±7	283±4	250±25
γ[mJ/mol·K^2]					
2.3±0.4	18±1	1.5±0.3	7±1	0.7±0.3	10±1

(ii) In low temperature region ($T<10$ K) the $C/T=f(T^2)$ curve for both ZrNiSn and HfNiSn samples exhibits unusual temperature dependence: a decrease in the value of γ about twice of its magnitude for ZrNiSn samples (Fig. 2) and with lower magnitude for HfNiSn (Fig. 3) as temperature decrease in the interval (10 – 3) K. We attribute this effect to the possible glass behavior in samples with small lattice disorder.

Figure 5 shows the low temperature part of the temperature dependences of the Seebeck coefficient S for three MNiSn (M = Ti, Zr, Hf) compounds treated in the same conditions (annealed in vacuum at 800 °C for 380 h). The temperature dependences $S(T)$ in temperature range ($10\text{ K}<T<800$ K) are presented in Fig. 7. The specific features of these curves are: anomalously high negative value of this quantity and their almost linear increase

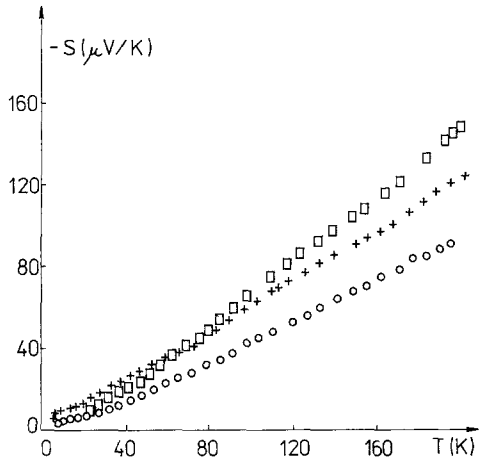

Fig. 5. Low temperature part of temperature dependences of Seebeck Coefficient $S(T)$ for TiNiSn (□), ZrNiSn (+), HfNiSn (○)

with temperature. The consideration of the next Section obtained in the simplest approximation within our band scheme assumption yield similar results.

Thermoelectric power of a single-band system of low electron (hole) concentration: results of relaxation time approximation

Consider for simplicity a single parabolic band and low electron (hole) concentration. If the standard relaxation time approximation time is used to describe the transport problem, the partial thermopower – corresponding to a single scattering process – is governed solely by a function of the electron (hole) fugacity $z=\xi(T)/kT$ [11, 12] found from the equation:

$$3(\varepsilon_F/kT)^{3/2}=2F_{1/2}(z), \tag{1}$$

where $F_n(z)$ is the Fermi-Dirac integral

$$F_n(z)=\int_0^\infty \mathrm{d}x\cdot x^n/\{1+\exp(x-z)\}, \tag{2}$$

ε_F the electron (hole) Fermi energy counted from the bottom (top of the band) and $\xi(T)$ its chemical potential. For the concentration of the current carriers of the order $10^{19}-10^{21}\,\mathrm{cm}^{-3}$, as in the compounds under consideration, and their effective mass equal to several free electron masses, the magnitude of ε_F is of the same order ($10^{-2}-10^{-3}$ eV) as in the typical semimetals. Then, the partial Seebeck coefficient can be computed from the formula (see, e.g., [11]):

$$S_r=(k/e)[(r+2)F_{r+1}(z)/(r+1)F_r(z)-z]. \tag{3}$$

The index r is here the scattering parameter characterizing the relaxation time energy dependence $\tau=\tau_0\varepsilon^{r-1/2}$. For the scattering by acoustic phonons $r=0$, optical phonons $r=1$, neutral impurities $r=1/2$ and charged ones $r=2$. The charge $e>0$ corresponds to holes and $e<0$ to electrons.

The standard approximations can hardly be applied for the solution of (1) in case of such a low electron concentration. This equation represents in fact the unique dependence $\xi(T)/\varepsilon_F$ as a function T/T_F (see, e.g., [13]). We are rather interested in the temperature dependence of z at a given low carrier concentration ($10^{19}-10^{21}\,\mathrm{cm}^{-3}$) and for the effective masses corresponding to a few free electron masses. Such dependences are shown by dash lines in Fig. 6. At low temperatures the standard asymptotic expansions ($z\to\infty, T\to\infty$) applied to $F_n(z)$ in (3) yields the Mott-Jones dependence $S\sim 1/z$, where z can be assumed as ε_F/kT. At higher temperatures, for $T>T_F$, the chemical potential and fugacity are negative. At sufficiently high temperatures ($T\geqq 10T_F$) the standard asymptotic expansion ($z\to\infty$) of the Fermi-Dirac integrals, used in the physics of semiconductors, can be applied. Since the first term in the square bracket in (3) yields a constant ($=2$ for $r=0$ and $(r+2)/r$ for $r=0$), the temperature behavior of S_r at high temperatures is simply described in terms of z by (const$-z$). This is obvious when comparing the solid and dash curves of Fig. 6.

The solid lines in Fig. 6 show the temperature dependence of S_r in units of k/e ($=86.2\,\mu V/K$) for $r=0$ (acoustic phonon scattering), derived from (1). The remaining parameters were assumed to have the following values: $m=2m_e$ (m_e = free electron mass), the electron (hole) concentration $n=10^{19}-10^{21}\,\mathrm{cm}^{-3}$ ($n=n_H$ of the experiment). The dash lines illustrate the corresponding temperature behavior of the fugacity $z=\xi(T)/kT$, resulting from the solution of (1). The corresponding values of the Fermi energy are: $8.46\cdot10^{-3}$ eV ($10^{19}\,\mathrm{cm}^{-3}$), $3.93\cdot10^{-2}$ eV ($10^{20}\,\mathrm{cm}^{-3}$), $1.82\cdot10^{-1}$ eV ($10^{21}\,\mathrm{cm}^{-3}$). Figure 7 shows the same dependence when the effective mass is doubled. For comparison we mark with the thick line an experimental dependence.

As seen from Figs. 6 and 7, made for acoustic phonon scattering ($r=0$), the magnitude of S_r at high temperatures is of the same order of magnitude as in the compounds under consideration and drastic changes in the electron (hole) concentration do not result in similar changes in the value of the Seebeck coefficient. The same conclusion can be drawn for other partial thermopowers since the temperature behavior of the first term in (3) is qualitatively the same for other values of r and its magnitude of the same order. Lowering of S_r at high temperatures is beyond this simple model. This may results from the temperature dependence of the chemical potential corresponding to a more realistic band shape. More sophisticated theory of low carrier density materials is also required. Basic assumptions and preliminary results for a system of overlapping bands are given in [14].

Final remarks

It is obvious that a real band structure, especially inside the gap, can be hardly described by a simple parabolic band. Our calculations of temperature dependences of Seebeck coefficient, taking into account only a high value

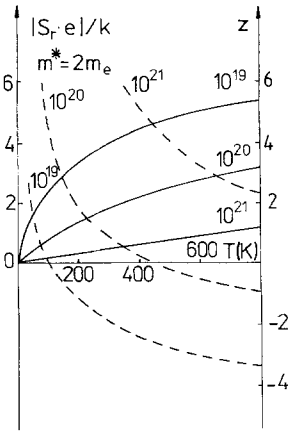

Fig. 6. Temperature dependence of S_r in units of k/e following from (1) and (3) (solid lines) and $z=\xi(T)/kT$ (dashed lines) for $m^*=2m_e$ and different electron (hole) concentrations

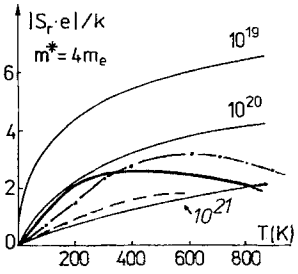

Fig. 7. The same dependence as in Fig. 6 when the effective mass is doubled. For comparison the experimental data up to high temperatures ($4<T<800$) K for TiNiSn (thick line), ZrNiSn (--*--) and HfNiSn (dashed line) samples are presented

of the effective mass $m^*\sim(2-4)m_e$ and small number of carriers $n_H\sim10^{20}$, describe experimental $S(T)$ data only at ($100<T<300$) K (see Fig. 6, 7). At $T>300$ K activation processes from E_F to E_c control the thermoelectric properties and S value decreases. Comparison of the experimental $S(T)$ data at high temperatures with the theoretical considerations of the previous section (Figs. 6, 7) allow us to get an estimation of the width of vacancy band Δ. We can assume that Δ is approximately equal to the value at which the experimental maximum of S is observed. Thus, as seen from Fig. 7 we have $\Delta\sim400$ K. At low temperatures ($T<100$ K), where the degeneracy occurs and activation effects are absent, theoretical results better correspond to the experimental ones if one will consider influence of localization with $E_F<E_c$ on transport properties, including thermoelectric power. It is worth to point out finally also that the temperature dependences of the Seebeck coefficients in MNiSn compounds are less sensitive to annealing than $\rho(T)$ data [3]. This empirical fact is confirmed by our calculations: a variation of n_H more than an order of magnitude lead to change of $S(200\,\mathrm{K})$ not more than by 30%.

To summaries we conclude that the assumed band structure scheme of the intermetallic vacancy compounds of MgAgAs structure (Fig. 1b) is sufficiently well supported by experimental data on the heat capacity and thermoelectric power. More precise estimations of m^* from $S(T)$ and the Hall effect data – based on a better theoretical approach and consideration of other scattering mechanisms – is planned.

We would like to acknowledge helpful discussions with Professors N.B. Brandt, I.P. Zvyagin, R. Troc, W. Suski and also to thank M.K. Zalyalutdinov, N.A. Samarin and Y.V. Stadnyk for their assistance in the experiment. We are also grateful to Professor S. Paszkowski for supplying precise numerical procedures for computing the Fermi-Dirac integrals.

References

1. De Groot, R.A., Mueller, F.M., Engen, P.G., Bushow, K.H.J.: Phys. Rev. Lett. **50**, 2024 (1983)
2. Van Engen, P.G., Bushow, K.H.J., Jongebreur, R.: Appl. Phys. Lett. **42**, 302 (1983)
3. Aliev, F.G., Brandt, N.B., Kozyrkov, V.V., Moshchalkov, V.V., Scolozdra, R.V., Stadnyk, Yu.V., Pecharskii, V.V.: Pis'ma Zh. Eksp. Teor. Fiz. **45**, 535 (1987)
4. Aliev, F.G., Belogorokhov, A.I., Brandt, N.B., Kozyrkov, V.V., Scolozdra, R.V., Stadnyk, Yu.V.: Pis'ma Zh. Eksp. Teor. Fiz. **47**, 151 (1988)
5. Aliev, F.G., Brandt, N.B., Moshchalkov, V.V., Kozyrkov, V.V., Scolozdra, R.V., Belogorokhov, A.I.: Z. Phys. B – Condensed Matter **75**, 167 (1989)
6. Kuriyama, K., Nakamura, F.: Phys. Rev. B **36**, 4439 (1987)
7. Fujii, H., Kawanaka, H., Takabatake, T., Kurisu, M., Yamaguchi, Y., Sakurai, J., Fujiwara, H., Fujita, T., Oguro, I.: J. Phys. Soc. Jpn. **58**, 2495 (1989)
8. Palstra, T.T.M., Nieuwenhuys, G.J., Vlastuin, R.M.F., Mydosh, J.A., Berg, J. van den, Bushow, K.H.J.: J. Magn. Magn. Mater. **67**, 331 (1987)
9. Daalderop, G.H.O., Mueller, F.M., Albers, R.C., Boring, A.M.: J. Magn. Magn. Mater **74**, 211 (1988)
10. Hanssen, K.E.H.M., Mijnarends, P.E.: Phys. Rev. B **34**, 5009 (1986).
11. Issi, J.P.: Austr. J. Phys. **32**, 1441 (1974)
12. Issi, J.P., Michenaaud, J.P., Heremans, J.: Phys. Rev. B **14**, 5136 (1976)
13. Julien, R., Beal-Monod, M.T., Coqblin, B.: Phys. Rev. B **9**, 1441 (1974)
14. Durczewski, K., Ausloss, M.: Phys. Rev. B (in press)